

High-temperature intrinsic ferromagnetism in heavily Fe-doped GaAs layers

A.V. Kudrin^{1,*}, V.P. Lesnikov¹, Yu.A. Danilov¹, M.V. Dorokhin¹, O.V. Vikhrova¹, P.B. Demina¹, D.A. Pavlov¹, Yu.V. Usov¹, Yu.M. Kuznetsov¹ and R.N. Kriukov¹

¹*Lobachevsky State University of Nizhny Novgorod, Gagarin av. 23/3, 603950 Nizhny Novgorod, Russia*

*kudrin@nifti.unn.ru

The layers of novel high-temperature diluted magnetic semiconductor (DMS) (Ga,Fe)As with the average Fe content up to 16 at. % were grown on (001) *i*-GaAs substrates using a pulsed laser deposition in a vacuum. The transmission electron microscopy and the energy-dispersive X-ray spectroscopy investigations revealed that the layers are epitaxial, do not contain any second-phase inclusions, but contains the columnar Fe-enriched regions. The layers can be characterized as the vertical periodic system consisting of the nano-columnar regions of (Ga,Fe)As DMS with higher Fe concentration separated by the regions of (Ga,Fe)As DMS with less Fe concentration. The *n*-type conductivity of the obtained (Ga,Fe)As layers apparently is associated with the formation of the Fe impurity band within the GaAs band gap. The hysteretic negative magnetoresistance was observed in the layers up to room temperature. The magnetoresistance investigations point to the out-of-plane magnetic anisotropy of the (Ga,Fe)As layers. The investigations of the magnetic circular dichroism confirm that the layers are intrinsic ferromagnetic semiconductors with the Curie point up to at least room temperature.

1. Introduction

Heavily Fe-doped diluted magnetic semiconductors (DMS) are promising materials for semiconductor spintronics, since the (Ga,Fe)Sb [1-4] and (In,Fe)Sb [5,6] DMSs with a Fe content up to 17 at. % and a room temperature (RT) Curie point have recently been created. At present, the nature of ferromagnetism in Fe doped narrow-gap ((In,Fe)As, (Ga,Fe)Sb, (In,Fe)Sb)) and wide-gap III-V ((Al,Fe)Sb) semiconductors is a subject of research. Apparently the ferromagnetism in (III,Fe)V DMSs is not carrier-mediated but related to some superexchange interaction between Fe atoms [5-8]. In particular, we recently observed a weak interrelation between the ferromagnetism and the charge carrier concentration in (In,Fe)Sb that is fundamentally different from Mn doped III-V DMSs [9]. Obtained results lead to the question about ability to create the ferromagnetic layers of a practically important semiconductor GaAs by introducing a large amount of Fe atoms (> 10 at. %) during an epitaxial growth.

There are a few papers from the early 2000s about the formation of the (Ga,Fe)As layers by molecular beam epitaxy (MBE) with a relatively low Fe content (up to 3.5 at. %). In the works [10-12] the Ga_{1-x}Fe_xAs layers with *x* in the range of 0.007 – 0.07 were grown at the temperatures in the range of 260 – 580°C. These layers were highly-resistive with a weak *n*-type conductivity. The structures obtained at 260 °C were characterized as Ga_{1-x}Fe_xAs homogeneous paramagnetic epilayers, whereas the structures obtained at 350 – 580 °C were GaAs epilayers with second-phase ferromagnetic inclusions. These (Ga,Fe)As layers were obtained at the relatively high temperatures and contained the relatively low amount of iron. Since by now both conductive ((In,Fe)As, (Ga,Fe)Sb, (In,Fe)Sb)) and insulating ((Al,Fe)Sb) ferromagnetic (III,Fe)V DMSs have been obtained, it

can be expected that the creation of ferromagnetic (Ga,Fe)As is also possible.

In this work we present the results of investigations of conductive (Ga,Fe)As layers with the ferromagnetic properties up to room temperature.

2. Experiments

The GaAs and (Ga,Fe)As layers were grown by a pulsed laser deposition (PLD) in a vacuum on semi-insulating (001) GaAs substrates [5,9,13]. The Fe content was set by the technological parameter $Y_{Fe} = t_{Fe}/(t_{Fe}+t_{GaAs})$, where t_{Fe} and t_{GaAs} are the ablation times of the Fe and GaAs targets, respectively.

The surface of the structures was investigated by an atomic force microscopy (AFM). The structural properties of the samples were investigated by an analytical transmission electron microscopy (TEM). The distribution of constituent elements was obtained by an energy-dispersive X-ray spectroscopy (EDS) during microscopy investigations. Optical reflectivity spectra were obtained at RT in the spectral range of 2.4 – 6 eV. The *dc* magnetotransport measurements were carried out in the van der Pauw and Hall bar geometry in a closed-cycle He cryostat. The investigations of the magnetic circular dichroism (MCD) were performed in the cryostat in the spectral range from 1.37 to 2.03 eV using a xenon arc lamp as a light source.

In this study we present results for the following structures: an undoped GaAs layer grown at 200 °C (sample 200-0, grown by the sputtering of the GaAs target only), and three (Ga,Fe)As layers with $Y_{Fe} = 0.08$, $Y_{Fe} = 0.17$, $Y_{Fe} = 0.25$ grown at 200 °C (samples 200-8, 200-17 and 200-25, respectively).

3. Results

3.1. Structural and optical properties

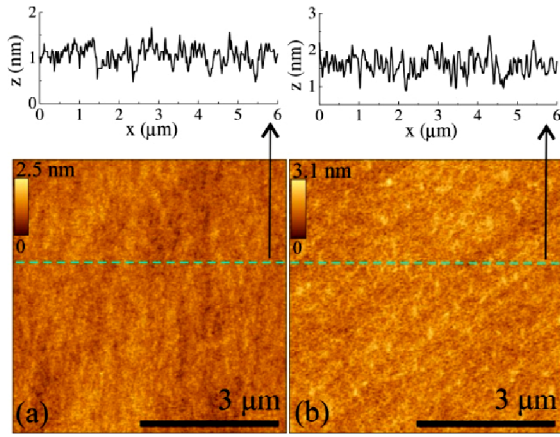


FIG. 1. AFM images and height profiles. (a) Structure 200-0. (b) Structure 200-25.

Figure 1 shows the AFM surface morphology of the structures 200-0 (Figure 1(a)) and 200-25 (Figure 1(b)). All obtained (Ga,Fe)As layers (and the GaAs layer) have the smooth surface with a root mean square (RMS) roughness of about 0.3 nm.

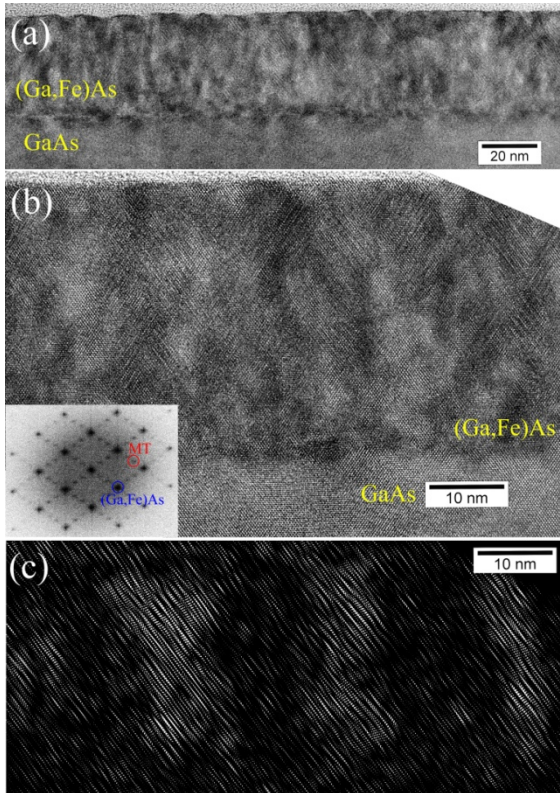


FIG. 2. Results of cross-section TEM investigations of (Ga,Fe)As/GaAs structure 250-25. (a) Overview TEM image of 200 nm long region. (b) HRTEM image of 75 nm long region (inset shows FFT diffraction pattern of image). (c) Inverse FFT image of (Ga,Fe)As layer obtained from MT (microtwin) spots of FFT diffraction pattern.

Figure 2(a) shows the overview TEM image from a 200 nm long region for the (Ga,Fe)As/GaAs structure 250-25. The image demonstrates a quite smooth (Ga,Fe)As layer with the thickness of about 35 nm without evident second-phase inclusions. Figure 2(b) shows a high-resolution TEM (HRTEM) image of a 75 nm long region for the structure 200-25. The

HRTEM image reveals a epitaxial character of the (Ga,Fe)As layer without evident second-phase inclusions. Earlier we reported that the (In,Fe)Sb layer obtained at a relatively high temperature (300 °C) contains Fe secondary phase clusters, that revealed on the HRTEM image as regions with a moiré-type contrast [13]. For the structure 250-25 the HRTEM image of the (Ga,Fe)As layer is free from any regions with a moiré-type contrast. At the same time the TEM images show a large number of stacking faults and microtwins along {111} planes, that appear as the assemblage of straight lines at an angle of $\approx 70^\circ$ with respect to each other (Figure 2(a) and 2(b)). The inset of Figure 2(b) shows a fast Fourier transform (FFT) diffraction pattern of the HRTEM image. The FFT diffraction pattern contains bright primary diffraction spots corresponding to a zinc-blende type lattice of the epitaxial (Ga,Fe)As matrix and additional spots between primary spots. The Figure 2(c) exhibits the inverse FFT image of the (Ga,Fe)As layer obtained from the additional spots of the FFT diffraction pattern. The comparison of the Figure 2(b) and Figure 2(c) reveals that the additional spots on the FFT diffraction pattern are related to the regions of the localization of the microtwins. Thus the additional diffraction spots are the consequence of the microtwins presence. The formation of stacking faults and microtwins in epitaxial layers is a consequence of the large lattice mismatch between different materials [5,14]. For GaSb and InSb matrices the introduction of a large number of Fe atoms leads to the lattice constant decrease [1,6]. Since the Fe atomic radius is less than the Ga and As atomic radius, the (Ga,Fe)As lattice constant should be less than the GaAs lattice constant. Apparently this is the cause of the microtwins appearance in the obtained (Ga,Fe)As layer. The regions of the microtwins localization have a columnar-shape with the width and period of about 10 nm (Figure 2(b) and Figure 2(c)). It can be assumed that these regions have the higher concentration of Fe atoms.

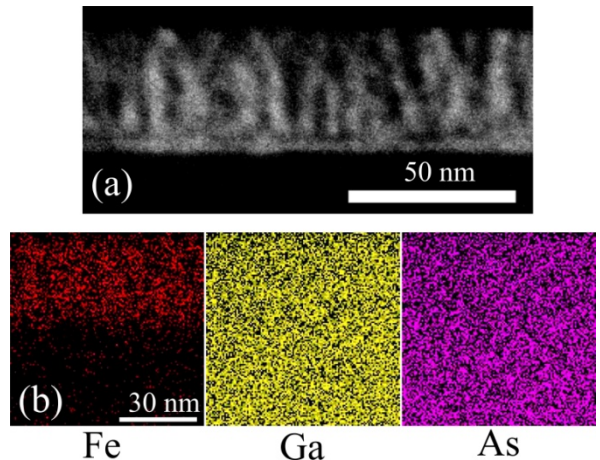


FIG. 3. (a) Z-contrast image of 135 nm long region for structure 200-25. (b) EDS mapping of Fe, Ga and As in (Ga,Fe)As layer.

Figure 3(a) presents a scanning cross-section TEM image in a high-angle annular dark-field

imaging mode (z-contrast image) of the structure 250-25. The periodic z-contrast image also confirms the presence of a periodic structure with a different atom densities. The bright areas in the z-contrast image are the areas with the higher concentration of more light atoms i.e. Fe-enriched regions. Figure 3(b) presents the EDS mapping of Fe, Ga and As atoms for the structure 200-25. The data reveal a rather uniform distribution of the elements within the (Ga,Fe)As layer, however the columnar Fe-enriched regions can be also observed on the Fe map. These results support the assumption that the columnar-shape regions of the microtwins localization have the higher concentration of the Fe atoms than the regions between them. Thus, the obtained (Ga,Fe)As layer of the structure 200-25 is a vertical periodic system consisting of the nano-columnar regions of (Ga,Fe)As DMS with higher Fe concentration separated by the regions of (Ga,Fe)As DMS with less Fe concentration. The similar structure with the nano-columnar Fe-enriched DMS region was observed in the 40-nm-thick $(\text{Ga}_{0.7}\text{Fe}_{0.3})\text{Sb}$ layer obtained by MBE on the AlSb buffer layer [4].

The EDS investigations show what the average Fe content in the (Ga,Fe)As layer for the structure 200-25 is about 16 ± 3 at.%. Taking into account this average Fe concentration for the structure 200-25 ($Y_{\text{Fe}} = 0.25$) and the technological Fe content for the structures 200-17 ($Y_{\text{Fe}} = 0.17$) and 200-8 ($Y_{\text{Fe}} = 0.08$), the average Fe concentration can be estimated as about 11 and 5 at.% for the structure 200-17 and 200-8, respectively.

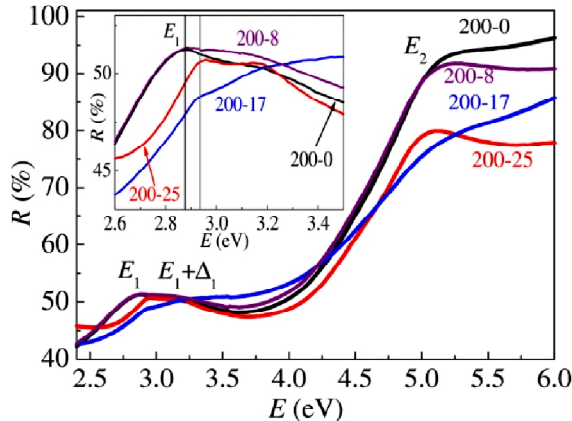


FIG. 4. Optical reflectivity spectra at 295 K for structures 200-0, 200-8, 200-17 and 200-25. Inset shows enlarged spectrum parts in E_1 region.

Figure 4 exhibits optical reflectivity spectra at 295 K for the structures 200-0, 200-8, 200-17 and 200-25. The reflectivity spectra for the (Ga,Fe)As layers agree with the spectrum for the undoped GaAs layer (the structure 200-0) and contain features associated with characteristic interband transitions for a bulk GaAs [15]. In particular, the doublet in the E_1 region and the intense peak in the E_2 region are observed. This indicates the conservation of the GaAs band structure for the (Ga,Fe)As layers.

For the structures 200-17 and 200-25 the E_1 peak has a clear blueshift. For the sample 200-25 the blueshift is larger (see the inset to Figure 4). The

blueshift of the E_1 peak position with the Fe concentration was observed earlier for the MBE and PLD $(\text{Ga,Fe})\text{Sb}$ [13,16] and $(\text{In,Fe})\text{Sb}$ layers [6,9].

3.2. Transport and magnetic properties

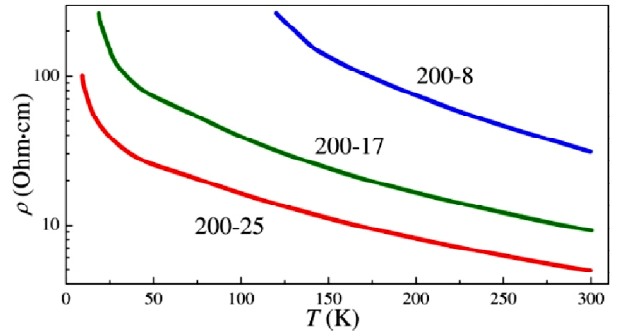


FIG. 5. Temperature dependences of resistivity for structures 200-8, 200-17 and 200-25.

Figure 5 shows the temperature dependences of a resistivity $\rho(T)$ for the structures 200-8, 200-17 and 200-25. The resistivity of the undoped GaAs layer (the structure 200-0) is comparable with the resistivity of the *i*-GaAs substrate. The $\rho(T)$ dependences are semiconductor type – the resistivity increases with decreasing temperature. The resistivity of the (Ga,Fe)As layers decrease with the Fe concentration increase. For the structures 200-8, 200-17 and 200-25 the Seebeck coefficient at room temperature corresponds to the *n*-type conductivity which is consistent with earlier works on the paramagnetic (Ga,Fe)As layers [10,11].

The obtained (Ga,Fe)As layers have the relatively high resistivity. The consequence of this is that the measured Hall resistance dependences on an external magnetic field ($R_{\text{MeasH}}(B)$) are completely determined by the dependences of the longitudinal resistivity on the external magnetic field (magnetoresistance) due to the nonideal Hall measurement geometry of the samples (both for the Hall bars and van der Pauw geometry). For our samples the true Hall resistance dependences on an external magnetic field (an odd function with respect to the B polarity) cannot be correctly extracted from the $R_{\text{MeasH}}(B)$ dependences. In this connection, we will analyse the magnetoresistance observed in the (Ga,Fe)As layers at different temperatures for the out-of-plane (B is applied perpendicularly to the sample plane) and in-plane (B is applied in the sample plane) orientations.

Figure 6(a) shows the magnetoresistance ($\text{MR} = (\rho(B) - \rho(0))/\rho(0)$) curves for the sample 200-25 at temperatures between 25 – 295 K with B is applied perpendicularly to the plane. A negative hysteretic MR is observed up to 295 K. At 25 and 75 K the out-of-plane MR curves do not saturate in the magnetic field of ± 0.35 T. For temperatures above 150 K the out-of-plane MR curves demonstrate the saturation at $B > 0.15 - 0.2$ T (Figure 6(a)). Figure 6(b) shows the MR curves for the sample 200-25 at various temperatures with B is applied in the plane. For the in-plane orientation the negative hysteretic MR is also observed up to 295 K. However

the shape of the MR curves at a given temperature is different for the out-of-plane and in-plane orientation. The MR measurements show that at 25 and 75 K the coercivity of the (Ga,Fe)As layer is higher for B is applied perpendicularly to the sample plane (Figure 6(b)).

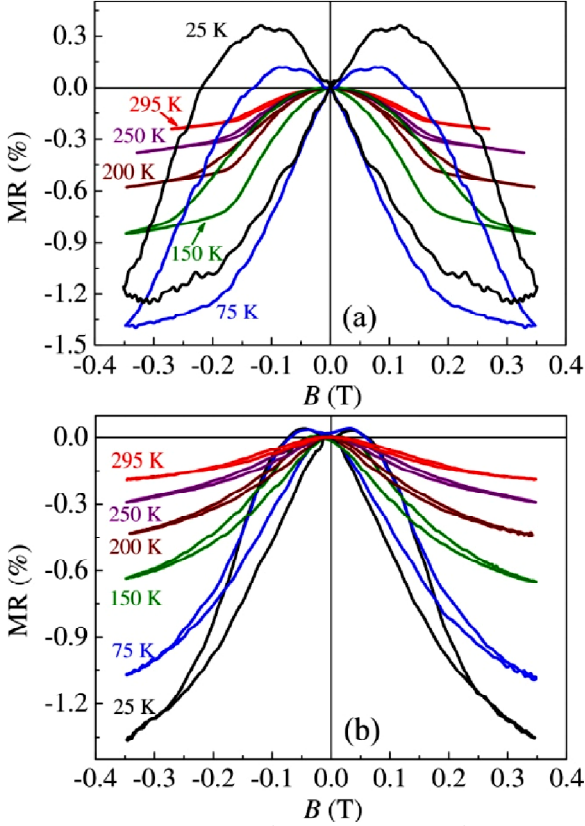


FIG. 6. MR curves at various temperatures for structure 200-25. (a) B is applied perpendicularly to sample plane. (b) B is applied in sample plane.

Also the MR investigations reveal that the magnetization of the (Ga,Fe)As layer easily saturates when B is applied perpendicularly to the sample plane (Figure 7). These results points to the out-of-plane magnetic anisotropy of the (Ga,Fe)As layer what is related to the presence of the columnar Fe-enriched $\text{Ga}_{1-x}\text{Fe}_x\text{As}$ regions. The observation of the hysteresis in the magnetoresistance up to 295 K reveals that the (Ga,Fe)As layer of the structure 250-25 has the Curie temperature (T_C) above RT.

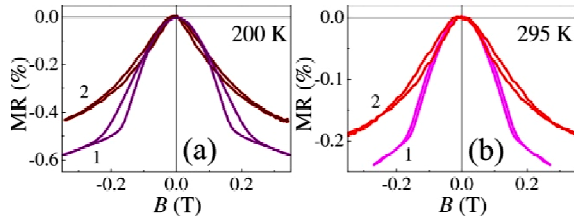


FIG. 7. MR curves for sample 200-25 at 200 K (a) and 295 K (b). 1 – B is applied perpendicularly to sample plane, 2 – B is applied in sample plane.

Figure 8(a) shows the MR curves for the sample 200-17 in the temperature range of 75 – 295 K with B is applied perpendicularly to the plane. As for the structure 200-25 the magnetoresistance is negative up

to 295 K but the hysteresis disappears at temperatures above 200 K (Figure 8). The out-of-plane MR curves also show that the coercivity of the (Ga,Fe)As layer for the structure 200-17 is smaller than that for the structure 200-25 (Figure 7) in the all temperature range. A comparison of the out-of-plane (Figure 8(a)) and in-plane (Figure 8(b)) MR curves at the given temperature also points to the out-of-plane magnetic anisotropy of the (Ga,Fe)As layer of the structure 200-17.

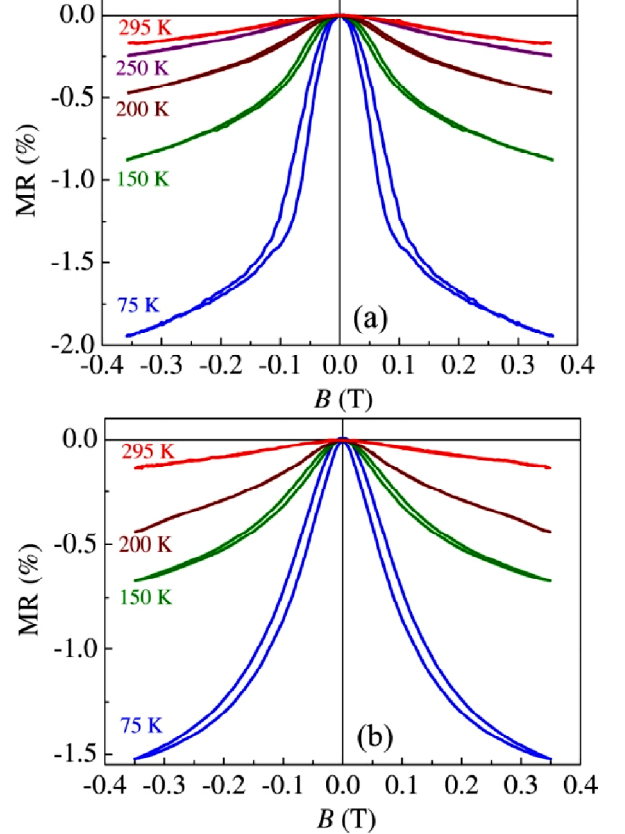


FIG. 8. MR curves at various temperatures for structure 200-17. (a) B is applied perpendicularly to sample plane. (b) B is applied in sample plane.

The out-of-plane MR curves for the structure 200-17 are hysteretic up to 200 K, hence its T_C is also about 200 K. The Fe concentration decrease leads to the weakening of the ferromagnetic properties of the (Ga,Fe)As layer and to T_C reduction.

For the structure 200-8 no reliable MR curves were obtained due to the higher resistance of the (Ga,Fe)As layer with the least Fe content.

To confirm that the ferromagnetic properties of the obtained layers are related to the intrinsic ferromagnetism of (Ga,Fe)As DMS, the studies of a magnetic circular dichroism were carried out for the structure 200-25 with T_C above RT. The MCD investigations were performed for B is applied perpendicularly to the sample plane. The light from a xenon arc lamp, after passing through a grating monochromator, was circularly polarized by the combination of a linear polarizer and an achromatic quarter-wave plate. The MCD value was defined as $((I^+ - I^-)/(I^+ + I^-)) \times 100\%$, where I^+ and I^- are the intensities of circularly polarized light with the right

and left circular polarization reflected from the sample's surface.

Figure 9 shows the MCD dependences on an external magnetic field ($MCD(B)$) for the structure 200-25 measured at 15 K for the photon energies in the range of 1.37 – 2.03 eV.

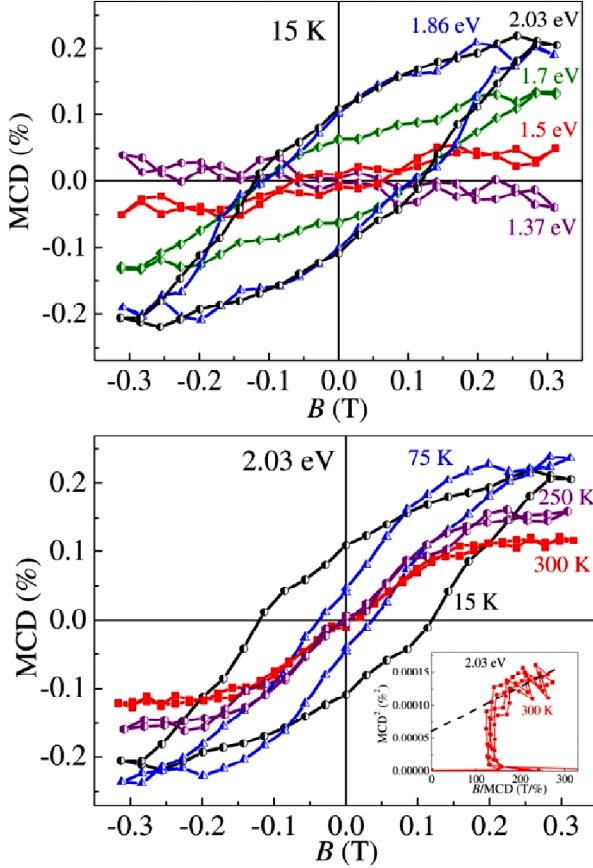


FIG. 9. (a) $MCD(B)$ dependences for structure 200-25 measured for different photon energies at 15 K. (b) $MCD(B)$ dependences for structure 200-25 at different temperatures for photon energy of 2.03 eV. Inset shows Arrot plot of $MCD(B)$ curve at 300 K.

For the photon energies of 2.03 and 1.86 eV that are notably higher than the GaAs band gap (E_g) at 15 K (~ 1.52 eV), the $MCD(B)$ dependences are hysteretic without the saturation and have the maximum amplitude (Figure 9(a)). Note that the hysteretic unsaturation shape of the $MCD(B)$ curves at 15 K is completely consistent with the out-of-plane MR curve at 25 K (Figure 6(a)). When the photon energy decreases to 1.7 eV the amplitude of the $MCD(B)$ dependence reduces. For the photon energy of 1.5 eV that is smaller than E_g of GaAs, the amplitude of the $MCD(B)$ dependence drops greatly. For the photon energy of 1.37 eV the detectable MCD effect practically absent (Figure 6(a)). The absence of the detectable MCD effect for the photon energies ≤ 1.5 eV (when GaAs becomes transparent) reveal that the observed ferromagnetic $MCD(B)$ curves (at the photon energies ≥ 1.7 eV) related to the intrinsic ferromagnetism of the (Ga,Fe)As layer but not to any second-phase Fe or intermetallic ferromagnetic inclusions. The spectral dependence of MCD also shows that the E_g of obtained (Ga,Fe)As layers is

close to E_g of GaAs. Figure 9(b) shows the $MCD(B)$ curves for the structure 200-25 for the photon energy of 2.03 eV in the temperature range of 15 – 300 K. The $MCD(B)$ curves confirm that the (Ga,Fe)As layer of the structure 200-25 is ferromagnetic up to RT (the inset of Figure 9(b) shows the Arrot plot of the $MCD(B)$ curve at 300 K). Thus the MCD investigations confirm that the (Ga,Fe)As layer of the structure 200-25 is diluted magnetic semiconductor with intrinsic ferromagnetic properties up to room temperature. Note that RT ferromagnetism in the structure 200-25 apparently is associated with the columnar Fe-enriched regions with the Fe content up to 25 at. % (Figure 2 and 3).

4. Discussion

The fabricated (Ga,Fe)As layers have the rather high resistivity but for the structures 200-25 and 200-17 the conductivity is also observed at low temperatures (Figure 5). This result is interesting in itself, since the Fe impurity forms deep acceptor level in the GaAs band gap (about 0.5 eV above the valence band (VB) edge [17,18]) and should be a compensating impurity. It could be expected that the conductivity of the heavily Fe-doped (Ga,Fe)As layers would be comparable to the conductivity of the semi-insulating GaAs. It is known, that for the high concentration of an impurity the formation of an impurity band (IB) is possible. In particular, 3d elements such as Mn and Ni form the acceptor IB [19]. The ferromagnetic properties and the current transfer in the (Ga,Mn)As DMS can be determined by charge carriers in the Mn impurity band separated from VB by a finite energy gap [20-23]. It was reported in the work [24] that in the ferromagnetic (Ga,Fe)Sb the Fe impurity forms the acceptor IB overlapping with VB and the Fe impurity band has a significant influence on the carrier transport. In the our (Ga,Fe)As layers, the Fe concentration is very high and the formation of the Fe impurity band can also be expected. Since Fe is the deep impurity, the formed IB should be separated from the VB. Therefore, the observed transport properties of the obtained (Ga,Fe)As layers are determined by the electron transport in the Fe-related IB. The mobility of the carriers localized within IB should be small (about or less than $1 \text{ cm}^2/\text{V}\cdot\text{s}$). Also, as it was shown by TEM and EDS studies, the periodic vertical structure with the different Fe concentration is observed within the (Ga,Fe)As layer (Figures 2 and 3). This should lead to the spatial inhomogeneity of the impurity band, to the strong modulation of the built-in electric field and consequently to the strong modulation the potential profile. These phenomena should further reduce the carrier mobility, which finally leads to the observed high resistivity of the structures. Taking into account the mobility of about $0.1 \text{ cm}^2/\text{V}\cdot\text{s}$ and the feature resistivity of $10 \text{ Ohm}\cdot\text{cm}$ (Figure 5), the carrier concentration of an order of magnitude of 10^{19} cm^{-3} can be obtained. This is much lower than the concentration of introduced Fe atoms. But this is possible, since the Fe acceptor forms the

deep empty acceptor IB in which the charge carriers (electrons) are delivered from some additional donor levels and the resulting concentration of conduction electrons can be much lower than the acceptor concentration. The observed ferromagnetism in the obtained (Ga,Fe)As layers with the Fe impurity band, in principle, can be associated with the Zener's double exchange model in which the exchange interaction is realized via carriers in the impurity band separated from the valence or conduction band [20]. However, the experimental studies of the conducting (Ga,Fe)Sb, (In,Fe)Sb and insulating (Al,Fe)Sb show that the ferromagnetism in these DMS is not related to the charge carriers but is determined by the some kind of superexchange interaction between Fe atoms. First-principle calculations for the Fe-doped III-V semiconductors showed that the occurrence of the differences in the majority-spin and minority-spin density of states is the common property of (III,Fe)V semiconductors [25,26]. Although the results of the first-principle calculation for (Ga,Fe)As were interpreted as the occurrence of the antiferromagnetic [25] or paramagnetic [26] state, we can assume that this is due to the imperfection of the used computational models and methods. Our presented results on the creation and study of the heavily Fe-doped (Ga,Fe)As layers definitely show that ferromagnetism (including at RT) may occurs in the (Ga,Fe)As system.

5. Conclusion

In summary, the conductive *n*-type (Ga,Fe)As layers with the average Fe content up to 17 at. % were obtained by the PLD method. The TEM and EDS investigations of the (Ga,Fe)As layer with the maximum Fe content revealed that the layer are epitaxial, does not contain any second-phase inclusions, but contains the columnar Fe-enriched regions. This layer can be characterized as the vertical periodic system consisting of the nano-columnar regions of (Ga,Fe)As DMS with higher Fe concentration separated by the regions of (Ga,Fe)As DMS with less Fe concentration. The conductivity of the (Ga,Fe)As layers apparently is associated with the formation of the Fe impurity band within the GaAs band gap. The hysteretic negative magnetoresistance were observed in the layers up to room temperature. The magnetoresistance investigations points to the out-of-plane magnetic anisotropy of the (Ga,Fe)As layers what is related to the presence of the columnar Fe-enriched $Ga_{1-x}Fe_xAs$ regions. The investigations of the magnetic circular dichroism confirm that the layers are intrinsic ferromagnetic semiconductors with the Curie point up to at least room temperature.

Thus, the possibility of creation of the conductive (Ga,Fe)As layers with the intrinsic ferromagnetic properties and the high Curie temperature was shown.

Acknowledgements

This study was supported by Russian Science Foundation (grant № 18-79-10088).

References

1. N. T. Tu, P. N. Hai, L. D. Anh, and M. Tanaka, High-temperature ferromagnetism in heavily Fe-doped ferromagnetic semiconductor (Ga,Fe)Sb, *Appl. Phys. Lett.* **108**, (2016) 192401.
2. Yu. A. Danilov, A. V. Kudrin, V. P. Lesnikov, O. V. Vikhrova, R. N. Kryukov, I. N. Antonov, D. S. Tolkachev, A. V. Alaferdov, Z. E. Kun'kova, M. P. Temiryazev, and A. G. Temiryazev, The study of features of formation and properties of A3B5 semiconductors highly doped with iron, *Phys. Sol. St.* **60**, (2018) 2176–2181.
3. S. Sakamoto, N. T. Tu, Y. Takeda, S. Fujimori, P. N. Hai, L. D. Anh, Y. K. Wakabayashi, G. Shibata, M. Horio, K. Ikeda, Y. Saitoh, H. Yamagami, M. Tanaka, A. Fujimori, Electronic structure of the high- T_C ferromagnetic semiconductor (Ga,Fe)Sb: X-ray magnetic circular dichroism and resonance photoemission spectroscopy studies, *Phys. Rev. B* **100**, (2019) 035204.
4. S. Goel, L. D. Anh, N. T. Tu, S. Ohya, M. Tanaka, In-plane to perpendicular magnetic anisotropy switching in heavily-Fe-doped ferromagnetic semiconductor (Ga,Fe)Sb with high Curie temperature, *Phys. Rev. B* **3**, (2019) 084417.
5. A. V. Kudrin, Yu. A. Danilov, V. P. Lesnikov, M. V. Dorokhin, O. V. Vikhrova, D. A. Pavlov, Yu. V. Usov, I. N. Antonov, R. N. Kriukov, A. V. Alaferdov, and N. A. Sobolev, High-temperature intrinsic ferromagnetism in the (In,Fe)Sb semiconductor, *J. Appl. Phys.* **122**, (2017) 183901.
6. N. T. Tu, P. N. Hai, L. D. Anh, M. Tanaka, High-temperature ferromagnetism in new *n*-type Fe-doped ferromagnetic semiconductor (In,Fe)Sb, *Appl. Phys. Exp.* **11**, (2018) 063005.
7. L. D. Anh, D. Kaneko, P. N. Hai, and M. Tanaka, Growth and characterization of insulating ferromagnetic semiconductor (Al,Fe)Sb, *Appl. Phys. Lett.* **107**, (2015) 232405.
8. N. T. Tu, P. N. Hai, L. D. Anh, M. Tanaka, Electrical control of ferromagnetism in the *n*-type ferromagnetic semiconductor (In,Fe)Sb with high Curie temperature, *Appl. Phys. Lett.* **112**, (2018) 122409.
9. A. V. Kudrin, V. P. Lesnikov, Yu. A. Danilov, M. V. Dorokhin, O. V. Vikhrova, D. A. Pavlov, Yu. V. Usov, I. N. Antonov, R. N. Kriukov, S. Yu. Zubkov, D. E. Nikolichev, A. A. Konakov, Yu. A. Dudin, Yu. M. Kuznetsov, M. P. Temiryazeva, N. A. Sobolev, Robustness of ferromagnetism in (In,Fe)Sb diluted magnetic semiconductor to variation of charge carrier concentration, *J. Mag. Mag. Mat.* **485**, (2019) 236–243.
10. S. Haneda, M. Yamaura, Y. Takatani, K. Hara, S. Harigae, H. Munekata, Preparation and Characterization of Fe-Based III-V Diluted Magnetic Semiconductor (Ga, Fe)As, *Jpn. J. Appl. Phys.* **39**, (2000) L9–L12.

11. S. Hirose, M. Yamaura, S. Haneda, K. Hara, H. MuneKata, GaFeAs: a diluted magnetic semiconductor grown by molecular beam epitaxy, *Thin Solid Films*, **371**, (2000) 272–277.
12. R. Moriya, Y. Katsumata, Y. Takatani, S. Haneda, T. Kondo, H. MuneKata, Preparation and magneto-optical property of highly-resistive (Ga,Fe)As epilayers, *Physica E* **10**, (2001) 224–228.
13. A. V. Kudrina, V. P. Lesnikov, D. A. Pavlov, Yu. V. Usov, Yu. A. Danilov, M. V. Dorokhin, O. V. Vikhrova, V. E. Milin, R. N. Kriukov, Yu. M. Kuznetsov, V. N. Trushin, N. A. Sobolev, Formation of epitaxial *p-i-n* structures on the basis of (In,Fe)Sb and (Ga,Fe)Sb diluted magnetic semiconductor layers, *J. Mag. Mag. Mat.* **487**, (2019) 165321.
14. N. Y. Jin-Phillipp, F. Phillipp, T. Marschner, W. Stolz, E. O. Göbel, Transmission electron microscopy study on defect reduction in GaAs on Si heteroepitaxial layers grown by metalorganic vapor phase epitaxy, *J. Cryst. Growth* **158**, (1996) 28–36.
15. R. R. L. Zucca and Y. R. Shen, Wavelength-Modulation Spectra of Some Semiconductors, *Phys. Rev. B* **1**, (1970) 2668.
16. N. T. Tu, P. N. Hai, L. D. Anh, M. Tanaka, Magnetic properties and intrinsic ferromagnetism in (Ga,Fe)Sb ferromagnetic semiconductors, *Phys. Rev. B*, **92**, (2015) 144403.
17. L. A. Hemstreet, Trends in the electronic properties of substitutional 3d transition-metal impurities in GaAs, *Phys. Rev. B*, **22**, (1980) 4590–4599.
18. E. Malguth, A. Hoffmann, M. R. Phillips, Fe in III–V and II–VI semiconductors, *Phys. Stat. Sol. (b)* **245**, (2008) 455–480.
19. W. J. Brown Jr., J. S. Blakemore, Transport and Photoelectrical Properties of Gallium Arsenide Containing Deep Acceptors, *J. Appl. Phys.* **43**, (1972) 2242.
20. K. Sato, L. Bergqvist, J. Kudrnovský, P.H. Dederichs, O. Eriksson, I. Turek, B. Sanyal, G. Bouzearar, H. Katayama-Yoshida, V.A. Dinh, T. Fukushima, H. Kizaki, R. Zeller, First-principles theory of dilute magnetic semiconductors, *Rev. Mod. Phys.* **82** (2010) 1633–1690.
21. M. Dobrowolska, K. Tivakornsasithorn, X. Liu, J.K. Furdyna, M. Berciu, K.M. Yu, W. Walukiewicz, Controlling the Curie temperature in (Ga, Mn)As through location of the Fermi level within the impurity band, *Nat. Mat.* **11** (2012) 444–449.
22. M. Kobayashi, I. Muneta, Y. Takeda, Y. Harada, A. Fujimori, J. Krempaský, T. Schmitt, S. Ohya, M. Tanaka, M. Oshima, V. N. Strocov, Unveiling the impurity band induced ferromagnetism in the magnetic semiconductor (Ga,Mn)As, *Phys. Rev. B* **89**, (2014) 205204.
23. A.V. Kudrin, O.V. Vikhrova, Yu.A. Danilov, M.V. Dorokhin, I.L. Kalentyeva, A.A. Konakov, V.K. Vasiliev, D.A. Pavlov, Yu.V. Usov, B.N. Zvonkov, The nature of transport and ferromagnetic properties of the GaAs structures with the Mn δ -doped layer, *J. Mag. Mag. Mat.* **478** (2019) 84–90.
24. K. Sriharsha, L. D. Anh, N. T. Tu, S. Goel, M. Tanaka, Magneto-optical spectra and the presence of an impurity band in p-type ferromagnetic semiconductor (Ga,Fe)Sb with high Curie temperature, *Appl. Phys. Lett. Mat.* **7**, (2019) 021105.
25. P. Zhang, Y. Kim, S. Wei, Origin of High-TC Ferromagnetism in Isovalent-Doped III-V Semiconductors, *Phys. Rev. Appl.* **11**, (2019) 054058.
26. S. Sakamoto, A. Fujimori, Densities of states in Fe-doped III-V semiconductors: a first-principles study, arXiv:1908.02311.